Asian Journal of Pharmaceutical Sciences 16 (2021) 120–128

Available online at www.sciencedirect.com

ScienceDirect

journal homepage: www.elsevier.com/locate/AJPS

Original Research Paper

Unraveling GLUT-mediated transcytosis pathway of glycosylated nanodisks

Huan Wang[a,b,c], *Zui Zhang*[a], *Juan Guan*[a,c], *Weiyue Lu*[c,d,*], *Changyou Zhan*[a,b,c,*]

[a] *Department of Pharmacology, School of Basic Medical Sciences and State Key Laboratory of Molecular Engineering of Polymers, Fudan University, Shanghai 200032, China*

[b] *Center of Medical Research and Innovation, Shanghai Pudong Hospital, Fudan University Pudong Medical Center, Shanghai 201399, China*

[c] *School of Pharmacy, Fudan University and Key Laboratory of Smart Drug Delivery (Fudan University), Ministry of Education and PLA, Shanghai 201203, China*

[d] *State Key Laboratory of Medical Neurobiology and MOE Frontiers Center for Brain Science, Institutes of Brain Science, Fudan University, Shanghai 200032, China*

ARTICLE INFO

Article history:
Received 6 May 2020
Revised 8 June 2020
Accepted 6 July 2020
Available online 27 July 2020

Keywords:
Blood-brain barrier
Transcytosis
Glucose transporter
Glycosylation
Lysosomal exocytosis

ABSTRACT

Glucose transporter (GLUT)-mediated transcytosis has been validated as an efficient method to cross the blood-brain barrier and enhance brain transport of nanomedicines. However, the transcytosis process remains elusive. Glycopeptide-modified nanodisks (Gly-A7R-NDs), which demonstrated high capacity of brain targeting via GLUT-mediated transcytosis in our previous reports, were utilized to better understand the whole transcytosis process. Gly-A7R-NDs internalized brain capillary endothelial cells mainly via GLUT-mediated/clathrin dependent endocytosis and macropinocytosis. The intracellular Gly-A7R-NDs remained intact, and the main excretion route of Gly-A7R-NDs was lysosomal exocytosis. Glycosylation of nanomedicine was crucial in GLUT-mediated transcytosis, while morphology did not affect the efficiency. This study highlights the pivotal roles of lysosomal exocytosis in the process of GLUT-mediated transcytosis, providing a new impetus to development of brain targeting drug delivery by accelerating lysosomal exocytosis.

1. Introduction

Blood-brain barrier (BBB) is an important physiological barrier to keep hemostasis by preventing the entry of toxic and unnecessary agents into the brain. Unfortunately, it presents a major obstacle to the brain transport of more than 98% small-molecule and 100% biomacromoleclar therapeutics [1]. The development of BBB permeable therapeutics remains an unmet clinical need [2].

* Corresponding author.
E-mail addresses: wylu@shmu.edu.cn (W.Y. Lu), cyzhan@fudan.edu.cn (C.Y. Zhan).
Peer review under responsibility of Shenyang Pharmaceutical University.

https://doi.org/10.1016/j.ajps.2020.07.001

Glucose transporter (GLUT) mediates the basal-level cellular uptake of glucose into brain and other organs. GLUT-mediated transcytosis has been validated as a successful strategy to cross the BBB and enhance brain transport therapeutics [3]. Glucose is a naturally occurring ligand of GLUT. After conjugation with drugs or nanomedicines, glucose and its analogs can facilitate brain transport via GLUT-mediated transcytosis [4,5]. However, the transcytosis process remains elusive. GLUT-mediated endocytosis, intracellular trafficking and exocytosis occur orderly to complete the transcytosis. Mechanistic understanding on these steps may be crucial to improve brain transport efficiency of GLUT-mediated transcytosis.

In our previous reports, glycosylated A7R peptide (Gly-A7R, A7R peptide is a phage display selected 7-mer peptide ligand of vascular endothelial growth factor receptor 2 and neuropilin-1 for glioma targeting) was modified on the surface of nanodisks (Gly-A7R-NDs), which recognized GLUT on the BBB to achieve efficient brain transport [6,7]. In the present work, Gly-A7R-NDs were utilized to better understand the whole transcytosis process. Endocytosis pathway, intracellular trafficking and exocytotic process of Gly-A7R-NDs were investigated in brain capillary endothelial cells (bEnd.3 cells), and the possible GLUT-mediated transcytosis process was depicted.

2. Materials and method

2.1. Materials and reagents

A7R peptide (ATWLPPR) and Gly-A7R were chemically synthesized via Fmoc-based solid-phase peptide synthesis as previously reported [7]. 1-palmitoyl-2-oleoyl-sn–glycero-3-phosphocho-line (POPC), 1,2-distearoyl-sn–glycero-3-phosphoethanolamine-N-[methoxy(polyethylene glycol)–2000] ($mPEG_{2000}$-DSPE) and cholesterol were purchased from A.V.T. Pharmaceutical, Co., Ltd. (Shanghai, China). 4′,6-diamidino-2-phenylindole (DAPI), 1,1′-dioctadecyl-3,3,3′,3′-tetramethylindodicarbocyanine (DiD, excitation/emission= 640/665 nm), 3,3′-dioctadecyloxacarbocyanine perchlorate (DiO, excitation/emission=480/520 nm), 1,1′-dioctadecyl-3,3,3′,3′ tetramethylindocarbocyanine perchlorate (DiI, excitation/emission=550/570 nm), ionomycin, chloroquine, LY294002, brefeldin A, monensin, nocodazole and paclitaxel (PTX) were acquired from Meilun Biology Technology Co. Ltd. (Dalian, China). Chloropromazine, filipin, mβ-cyclodextrin (mβCD), genistein, colchicine and cytochalasin D were from Sigma-Aldrich (St. Louis, USA). Golgi-Tracker Green (BODIPY® FL C5-Ceramide), ER-Tracker Green, MitoTracker® Green FM, LysoTracker Green, Goat Anti-Rabbit IgG-FITC (H + L) were purchased from Yeasen Biotech Co., Ltd. (Shanghai, China). Anti-Rab11 (ab3612), anti-Rab8A (ab188574), rabbit anti-EEA1 (ab2900) and anti-M6PR (ab2733) antibody were obtained from Abcam (Cambridge, USA). bEnd.3 cell line was from Shanghai Institute of Cell Biology. Cells were cultured in Dulbecco's Modified Eagle Medium (DMEM, Gibco) containing 10% fetal bovine serum (FBS, Gibco) at 37 °C under a humidified atmosphere with 5% CO_2.

2.2. Preparation and characterization of glycopeptide modified nanodisks

Gly-A7R-NDs, FITC-labeled Gly-A7R-NDs (Gly-A7R-NDs-FITC), DiD-loaded Gly-A7R-NDs (Gly-A7R-NDs/DiD) and PTX-loaded Gly-A7R-NDs (Gly-A7R-NDs/PTX) were prepared as described previously [6,7]. For example, a mixture of the desired materials (POPC/cholesterol/$mPEG_{2000}$-DSPE/^{9}G-A7R-PEG_{3400}-DSPE at a molar ratio of 35:40:23:2) was dissolved in chloroform and rotary evaporated to form a thin film, which was hydrated in phosphate buffered saline (PBS) for the preparation of Gly-A7R-NDs. The hydrated solution was sonicated for 45 min in an ice-bath using a JY92-II sonicator (Scientz, Ningbo, China). Any precipitates were removed by filtrating through a membrane of 0.22 μm pore size. The nanodisks modified only with A7R peptide (no glycosylation, A7R-NDs) were prepared using the same method except for the change of lipid to POPC/cholesterol/$mPEG_{2000}$-DSPE/A7R-PEG_{3400}-DSPE at a molar ratio of 35:40:23:2. The liposomes modified with A7R peptide (no glycosylation, A7R-LSs) were prepared with the lipid composition of POPC/cholesterol/$mPEG_{2000}$-DSPE/A7R-PEG_{3400}-DSPE at a molar ratio of 55:40:3:2.

The morphology of Gly-A7R-NDs was characterized using a FEI Tecnai G20 transmission electron microscope (Cryo-EM, FEI, Hillsboro, USA). Size (diameter, nm) and polydispersity index (PDI) were measured using a Zen 3600 Zetasizer (Malvin, USA).

The stability of Gly-A7R-NDs was evaluated using SDS-polyacrylamide gel electrophoresis (SDS-PAGE) and fluorescence imaging method [8]. Briefly, Gly-A7R-NDs-FITC were incubated with PBS, 10% FBS, 10% mice serum, 5% Triton X-100 at 37 °C or with PBS at 4 °C for 4 h, and separated using 8% semi-native polyacrylamide gel. The sample was subject to imaging using an *in vivo* imaging system (IVIS Spectrum, Caliper, USA, excitation/emission= 480/520 nm).

2.3. Cellular uptake

The uptake of Gly-A7R-NDs by bEnd.3 cells was investigated using Förster resonance energy transfer (FRET) method as previously reported [9]. Three fluorescent dyes DiO, DiI and DiD at a mass ratio of 2:2:1 co-loaded in Gly-A7R-NDs (Gly-A7R-NDs/DiO/DiI/DiD) or only DiO (Gly-A7R-NDs/DiO) were prepared by the thin-film hydration and extrusion method [9] bEND.3 cells were seeded into confocal chambers at a density of 2×10^4 cells per well and incubated with Gly-A7R-NDs/DiO/DiI/DiD or Gly-A7R-NDs/DiO at the same fluorescence intensity at 37 °C for 2 h, 4 h, 8 h and 12 h, respectively. Cells were fixed with 4% formaldehyde and the nuclei were stained with DAPI. Intracellular fluorescence was visualized using a laser scanning confocal microscope (TCS SP5, Leica, Germany).

2.4. Endocytosis pathway assay

To investigate the internalization mechanism of Gly-A7R-NDs, bEnd.3 cells were pre-incubated with various inhibitors (as shown in Table S1) at 37 °C for 30 min, followed by incubation

with Gly-A7R-NDs/DiD (10 μg/ml of DiD) at 37 °C for 1 h. The treated cells were trypsinized and suspended in PBS, and the mean fluorescence intensity was quantified by flow cytometer (CytoFlex S, Beckman, USA). The relative cell uptake rate was calculated using the cells treated with blank culture medium as the negative control.

2.5. *Intracellular localization*

Immunofluorescence assay was used for subcellular location of Gly-A7R-NDs. Briefly, after pre-incubation with Gly-A7R-NDs/DiD, bEnd.3 cells were incubated with the following primary antibodies, such as EEA1, M6PR, Rab11 and Rab8a. FITC labeled secondary antibodies were used to detect the primary antibodies. The fluorescent images were captured using a laser scanning confocal microscope (TCS SP5, Leica, Germany) after washing, fixation with 4% paraformaldehyde and DAPI staining. For organelles co-localization, bEnd.3 cells were incubated with the Golgi-Tracker Green, ER-Tracker Green, MitoTracker® Green FM and LysoTracker Green instead of the aforementioned antibodies.

2.6. *Exocytosis pathway*

bEnd.3 cells were incubated with Gly-A7R-NDs/DiD for 4 h, then washed with PBS and incubated with the blank culture medium or various inhibitors (as shown in Table S2) for 2 h, 8 h and 24 h, respectively. The cells were trypsinized and the intracellular fluorescence intensity was measured using a flow cytometer (CytoFlex S, Beckman, USA). A7R peptide modified nanodisks (A7R-NDs/DiD) and liposomes (A7R-LSs/DiD) were used to investigate the effect of glycosylation and morphology on exocytosis.

Exocytosis pathway was investigated by measuring the cytotoxicity of Gly-A7R-NDs/PTX. bEnd.3 cells were incubated with Gly-A7R- NDs/PTX (1 ng/ml of PTX) for 4 h at 37 °C. The culture medium was replaced with the inhibitors for another 4 h (Chloroquine, 40 μM; LY294002, 20 μM; Nocodazole, 5 μg/ml; Brefeldin A, 20 μg/ml; Monensin, 20 μg/ml). The cells were washed with PBS and incubated with the blank culture medium for 64 h. Cell viability was measured by MTT assay.

2.7. *Statistical analysis*

Data were as means ± SDs from the sample numbers (n). Data from experiments were analyzed with GraphPad Prism 6.0. A two-sided Student's t-test with unpaired comparisons was used to evaluate differences in comparison of two groups. One-way ANOVA was used to test differences in comparison of groups more than two. $p < 0.05$ was considered statistically signifcant (ns: $P > 0.05$, $^{*}P < 0.05$, $^{**}P < 0.01$, $^{***}P < 0.001$).

3. Results and discussion

3.1. *Characterization of Gly-A7R-NDs*

The morphology and size of Gly-A7R-NDs were characterized using Cryo-EM and dynamic laser scattering (DLS). As shown in Fig. 1A, Gly-A7R-NDs have flat circular phospholipid bilayers surrounded by a PEGylated edge. Gly-A7R-NDs exhibited discoidal structure with a length of 50 nm in the Cryo-EM micrograph (Fig. 1B). Hydrodynamic diameter of Gly-A7R-NDs was about 60 nm with a polydispersity (PDI) of 0.254 (Fig. 1C and D), which was consistent with our previous report [6,7]. A7R-NDs had similar size around 60 nm (Fig. S1), suggesting that glycosylation did not affect the size and polydispersity of nanodisks. Gly-A7R-LSs and A7R-LSs with the diameter of 60 nm (Fig. S1) were prepared to study the effect of morphology on transcytosis. To study the stability in serum, Gly-A7R-NDs-FITC were incubated with PBS, 10% FBS, 10% mice serum or 5% Triton X-100 at 37 °C for 4 h, respectively. The mixture was subject to SDS-PAGE separation. As shown in the lane #5 of Fig. 1E, the fluorescence band of Gly-A7R-NDs-FITC treated with 5% Triton X-100 shifted forward. In contrast, Gly-A7R-NDs-FITC exhibited high stability in 10% FBS (lane #3) and 10% mice serum (lane #4) since fluorescent bands did not move.

3.2. *Multiple pathways are involved in the endocytosis of Gly-A7R-NDs*

To study the intracellular stability of nanodisks, three fluorescent probes were entrapped in Gly-A7R-NDs. The FRET effect was used to investigate the integrity of Gly-A7R-NDs during cellular uptake. In principle, when the Gly-A7R-NDs/DiO/DiI/DiD were intact and irradiated with 480 nm laser light, energy could be transferred from DiO to DiD to emit long wave-length fluorescence. As shown in Figs. 2A and S2, Gly-A7R-NDs/DiO/DiI/DiD emitted obvious FRET fluorescence excited by DiO at 480 nm after different times of incubation. The individual fluorescence of DiO and DiD also completely overlapped. In contrast, Gly-A7R-NDs/DiO showed no FRET fluorescence. These results validated the intracellular integrity of Gly-A7R-NDs.

The endocytosis was investigated by using a variety of inhibitors that can block different endocytic pathways [10]. As shown in Fig. 2B, chlorpromazine and hypertonic sucrose that can inhibit clathrin-related endocytosis significantly reduced the uptake of Gly-A7R-NDs in bEnd.3 cells, suggesting the involvement of clathrin-mediated endocytosis of Gly-A7R-NDs. However, caveolin-associated endocytosis was excluded in the endocytic pathway. Philipin and genistein did not effectively inhibit the cellular uptake. High concentration (0.55 M) of glucose could reduce the uptake of Gly-A7R-NDs, suggesting GLUT was at least partially involved in the endocytic pathway. In addition, the internalization of Gly-A7R-NDs could be inhibited by colchicine (macropinocytosis inhibitor), indicating that macropinacytosis was involed. The internalization was inhibited at low temperature (4 °C), indicating that energy was needed. These results validated that the endocytosis of Gly-A7R-NDs was mediated by multiple pathways, such as clathrin/GLUT-mediated endocytosis and energy-dependent macro-pinocytosis pathway.

3.3. *Intracellular trafficking of Gly-A7R-NDs*

After endocytosis, nanodisks are merged with endosome network and sorted for different cellular fates. Generally,

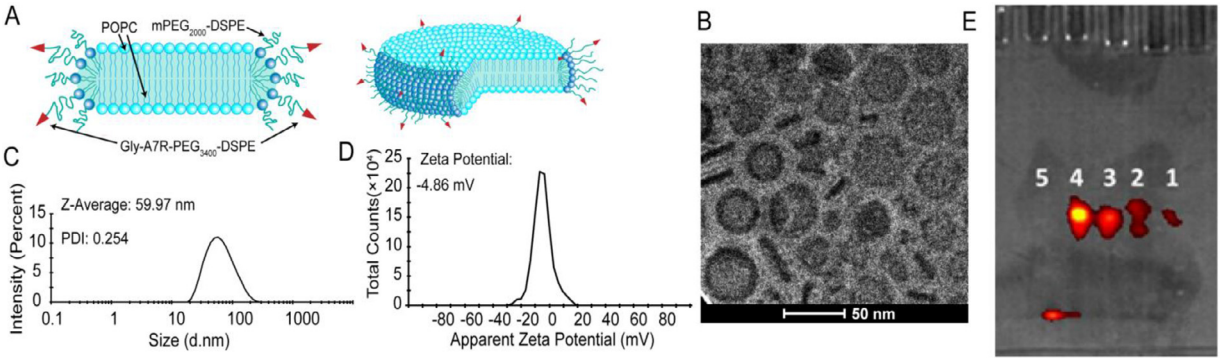

Fig. 1 – Characterization of Gly-A7R-NDs. (A) Schematic diagram of Gly-A7R-NDs. Spatial structures: upper; Planar structures: lower. (B) Cryo-EM micrograph of Gly-A7R-NDs. The arrow and arrowhead indicated the frontal and lateral views of Gly-A7R-NDs, respectively. The hydrodynamic diameter (C) and zeta potential (D) of Gly-A7R-NDs measured using DLS. Gly-A7R-NDs displayed a hydrodynamic diameter around 60 nm and slightly negative surface charge (−4.86 mV). (E) SDS-PAGE and fluorescence image of Gly-A7R-NDs-FITC. Gly-A7R-NDs-FITC were incubated with (1) PBS at 4 °C, (2) PBS at 37 °C, (3) 10% FBS at 37 °C, (4) 10% ICR mice serum at 37 °C or (5) 5% Triton at 37 °C for 4 h. In triton, the nanodisks were disrupted and the dye was shifted forward. Gly-A7R-NDs were stable under all other conditions.

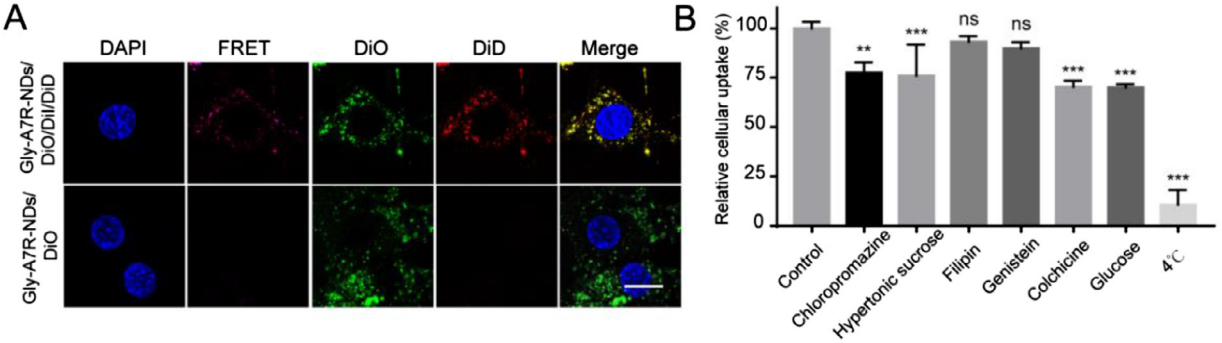

Fig. 2 – Endocytic pathways of Gly-A7R-NDs by bEnd.3 cells. (A) Confocal micrographs of cells incubated with Gly-A7R-NDs/DiO/DiI/DiD or Gly-A7R-NDs/DiO at 37 °C for 12 h. Gly-A7R-NDs efficiently internalized into bEnd.3 cells and remained intact. Scale bar = 10 μm. (B) The effect of a variety of inhibitors that can block different endocytic pathways on cellular uptake using a flow cytometer. Cells treated with the blank medium represented the control and the intracellular fluorescence intensity was set as 100%. All data were statistically analysed using ANOVA (ns indicates non-significant, $^{**}P < 0.01$, $^{***}P < 0.001$); Mean ± SD, $n = 3$.

they are mainly delivered to the lysosomes for degradation, recycled to plasma membrane or sorted to the trans-Golgi network for transcytosis in polarized cells. Rab GTPases play key roles in regulating the membrane trafficking and the compartmentalization of the endo-membrane system. More than 30 Rab proteins have been identified as vesicle trafficking markers [11–14]. To track the intracellular trafficking of Gly-A7R-NDs, we detected the co-localization between Gly-A7R-NDs/DiD and markers of classic endo-compartments and organelles.

Considering clathrin-mediated endocytosis always directs nanoparticles to the lysosomes [15,16], we investigated the co-localization of Gly-A7R-NDs with early endosomes (EE), late endosomes (LE) and lysosomes. Early endosome antigen 1 (EEA1) and mannose-6-phosphate receptors (M6PR) are widely used markers for EE and LE in the endocytic pathway studies, respectively [17]. As shown in Figs. 3A and S3, co-localization of Gly-A7R-NDs with EE could be observed at the early stage (1 h). With the prolongation of incubation duration, Gly-A7R-NDs were increasingly transferred from EE to LE (Figs. 3B and S4). After 12 h incubation, a majority of intracellular Gly-A7R-NDs were found to be co-localized with lysosomes labeled with LysoTracker Green probe (Figs. 3C and S5). These data demonstrated the transport of Gly-A7R-NDs via the classic EE-LE-Lysosomes endocytic pathway. In addition, Gly-A7R-NDs co-localized well with Rab11-labeled RE after 1 h incubation as shown in Figs. 3D and S6, indicating that Gly-A7R-NDs could be transported out of the cells through slow recycling endosomes (RE) pathways [12,13].

Golgi apparatus is one of the endometrial systems of eukaryotic cells, consisting of saccules, vacuoles and vehicles. Internalized cargos are secreted out from cells through vehicles [18,19]. The co-localization of Gly-A7R-NDs with golgi apparatus was shown in Figs. 3E and S7. Golgi apparatus

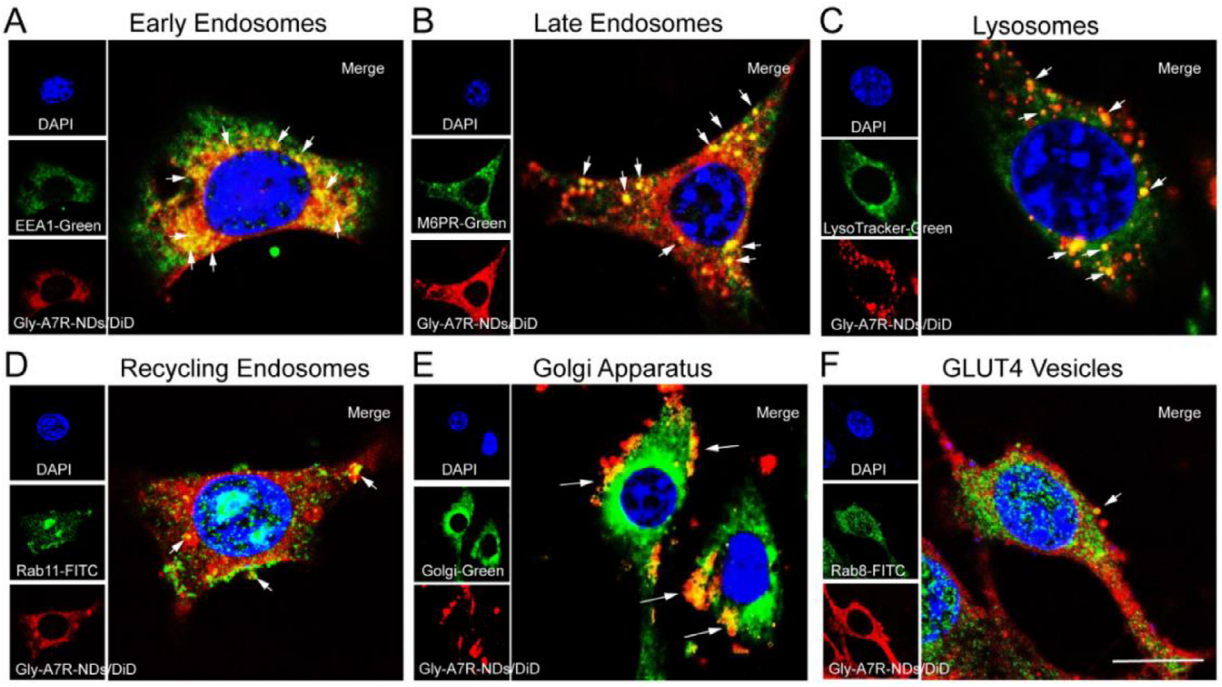

Fig. 3 – Intracellular trafficking of Gly-A7R-NDs in bEnd.3 cells. Co-localization of Gly-A7R-NDs with early endosomes marked with EEA1 at 1 h (A), late endosomes marked with M6PR at 4 h (B), lysosomes at 12 h (C), recycling endosomes marked with Rab11 at 1 h (D), Golgi apparatus at 4 h (E) and GLUT4 vesicles marked with Rab8 at 4 h (F), respectively. Blue: nuclei; Red: Gly-A7R-NDs/DiD; Green: Different intracellular compartments or markers. Scale bar = 10 μm.

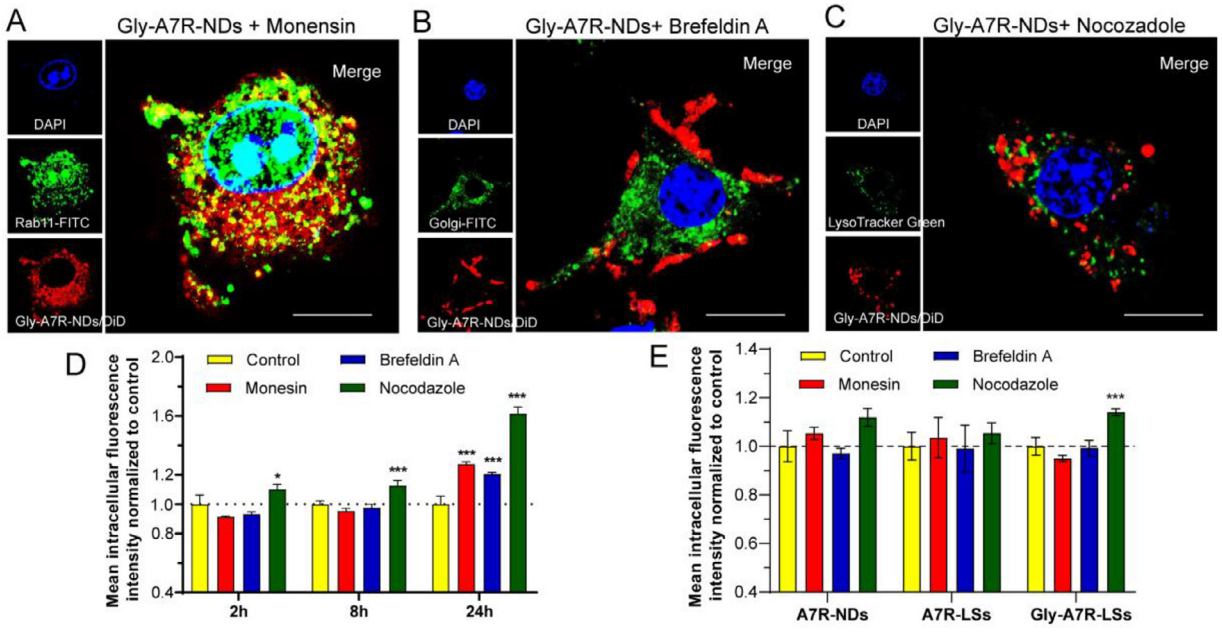

Fig. 4 – Exocytic pathway of Gly-A7R-NDs from bEnd.3 cells. (A) Co-localization of Gly-A7R-NDs and recycling endosomes treated with monensin at 37 °C for 2 h. (B) Co-localization of Gly-A7R-NDs and Golgi apparatus treated with brefeldin A at 37 °C for 4 h. (C) Co-localization of Gly-A7R-NDs and lysosomes treated with nocozazole at 37 °C for 8 h. Scale bar = 10 μm. The influence of exocytosis related inhibitors on intracellular (D) Gly-A7R-NDs, (E) A7R-NDs, A7R-LSs and Gly-A7R-LSs during co-incubation. Cells treated with blank medium represented the control and the intracellular fluorescence intensity was set as 100%. All data were statistically analysed using ANOVA (*$P < 0.05$, ***$P < 0.001$). Data are mean ± SD, $n = 3$.

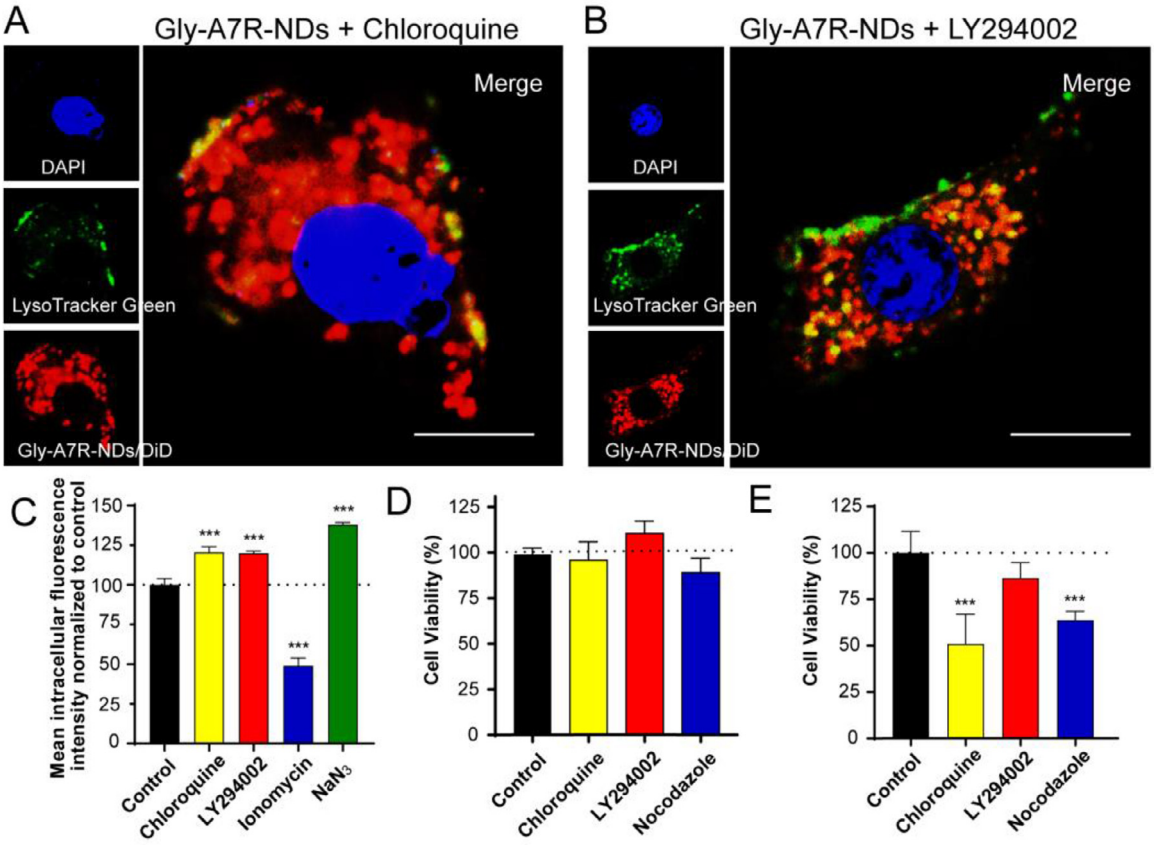

Fig. 5 – Effect of lysosomal exocytosis on efflux of Gly-A7R-NDs by bEnd.3 cells. Co-localization of Gly-A7R-NDs with lysosomes treated with chloroquine (A) or LY294002 (B) at 37 °C for 8 h. (C) The influence of lysosomal exocytosis related inhibitors on intracellular Gly-A7R-NDs during co-incubation. Cells treated with blank medium represented the control and the intracellular fluorescence intensity was set as 100%. (D) Cytotoxicity of free lysosomal exocytosis-related inhibitors on bEnd.3 cells. (E) The effect of lysosomal exocytosis related-inhibitors on cytotoxicity of Gly-A7R-NDs/PTX on bEnd.3 Cells for 72 h incubation (*$P < 0.05$, ***$P < 0.001$ v.s. Control, mean ± SD, $n = 3$).

distributed along the nucleus and the vehicles dispersed through the cytoplasm. Gly-A7R-NDs co-localized with golgi vehicles well, suggesting that golgi apparatus was involved in the secretion of Gly-A7R-NDs. GLUT4 transport vehicles are derived from the trans-Golgi network [11,12,20]. In order to examine whether Gly-A7R-NDs could be secreted out of the cells through the GLUT4 vehicles pathway, we labeled the GLUT4 vehicles with Rab8 and found that Gly-A7R-NDs began to co-localize obviously after 2 h of incubation with cells (Figs. 3F and S8). The results demonstrated that Gly-A7R-NDs should be transported into the Golgi and then sequestered in GLUT4 transport vesicles to complete transcytosis. We did not observe co-localization of Gly-A7R-NDs with other organelles like endoplasmic reticulum and mitochondrion as shown in Fig. S9.

3.4. *Lysosomal exocytic pathway plays important roles in exocytosis of Gly-A7R-NDs*

The intracellular trafficking of Gly-A7R-NDs indicated that the potential exocytosis pathways could be recycling endosomes secretion, golgi secretion and lysosomal exocytosis. Gly-A7R-NDs could be exocytosed through golgi secretion and/or lysosomal exocytosis. To investigate the exocytic process, a variety of inhibitors (as shown in Table S2) that can block different exocytic pathways were utilized.

Monensin is a golgi/RE exocytosis pathway related inhibitor [21,22] and the recycling endosomes together with Gly-A7R-NDs were retained in the cells by monensin (Fig. 4A). Brefeldin A is a compound that can inhibit protein exocytosis by causing collapse of the Golgi apparatus [23,24], and the dispartation of Gly-A7R-NDs with golgi could clearly been seen in Fig. 4B. Lysosomes play key roles in eliminating the internalized nanoparticles by degradation, dissolution or exocytosis [25]. Lysosomal exocytosis refers to the fusion of the lysosomal membrane with the plasma membrane, resulting in the secretion of lysosome components out of the cell [26,27]. In addition to golgi-related secretion, lysosomal exocytosis might be the main routes of nanoparticles for transcytosis [26]. Nocodazole is a microtubule related inhibitor and the microtubule formation is required for transport of the lysosomes to the periphery and fusion with the plasma membrane [27,28]. The use of nocodazole caused Gly-A7R-NDs to escape from the lysosomes (Fig. 4C).

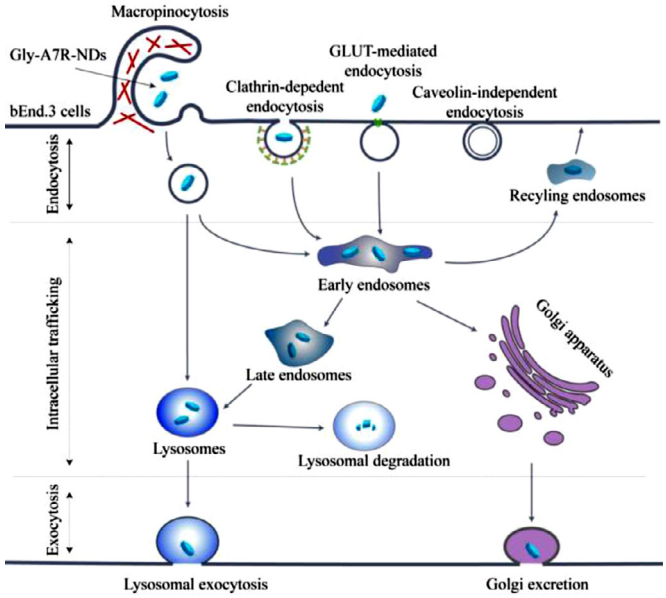

Fig. 6 – Schematic representation of the transcytosis pathways of Gly-A7R-NDs in bEnd.3 cells.

In order to investigate the effect of recyling endosmes, golgi apparatus and lysosomes on the exocytosis, the intracellular fluorescence intensity of Gly-A7R-NDs/DiD after the treatment of respective inhibitors (monensin, brefeldin A and nocodazole) was measured by flow cytometry (Fig. 4D). Monensin and brefeldin A did not prevent the exocytosis of Gly-A7R-NDs at 2 h and 8 h. Only after 24 h of incubation, the intracellular fluorescence intensity was 1.21 and 1.27 times that of the control group, respectively. In contrast, nocodazole significantly inhibited the efflux of Gly-A7R-NDs. The intracellular fluorescence intensity after 2 h, 8 h, and 24 h were 1.10, 1.13 and 1.61 times that of the control group, respectively. The results suggested the important roles of lysosomal exocytosis in the transcytosis of Gly-A7R-NDs.

The exocytosis pathway of nanodisks without glycosylation (A7R-NDs), liposomes with glycosylation (Gly-A7R-LSs) and liposomes without glycosylation (A7R-LSs) were also investigated (Fig. 4E). In comparison to Gly-A7R-NDs, none of the aforementioned inhibitors had significant effects on the exocytosis of A7R-NDs, indicating A7R-NDs might be exocytosed from cells in a non-specific pathway. Nocodazole significantly inhibited the efflux of Gly-A7R-LSs, similar to that of Gly-A7R-NDs. In addition, A7R-LSs exhibited non-specific exocytic pathway like A7R-NDs. Results indicat that not morphology but glycosylation had key roles of exocytosis of lipid-based nanoparticles.

GLUT8 (facilitated glucose transporter, member 8) was found to contain a highly conserved late endosomal/lysosomal motif and was observed within endosomal/lysosomal membranes [29,30]. There are increasing evidences suggesting that the most plausible intracellular localization of GLUT8 is its association with lysosomes [31–33]. Glycosylation could facilitate more Gly-A7R-NDs to enter the lysosomes than A7R-NDs, which might explain Gly-A7R-NDs were secreted mainly through lysosomal exocytosis. Similar to A7R-NDs, the exocytosis pathway of A7R-LSs was also not effected by inhibitors, suggesting that morphology of lipid-based nanoparticles had ignorable effects on the exocytosis (Fig. 4E).To further understand the involvement of lysosomes in exocytosis of Gly-A7R-NDs, a series of lysosomal exocytosis related reagents (Table S2) were used to investigate exocytosis of Gly-A7R-NDs. Chloroquine is capable of inhibiting the activity of lysosomal enzymes and has been widely used for lysosomal escape [27,34]. Chloroquine significantly decreased the co-localization of Gly-A7R-NDs with lysosomes (Fig. 5A), resulting in Gly-A7R-NDs retention in cells and the intracellular fluorescence intensity was much higher than that of the control group (Fig. 5C). Lipid kinase PIK3 plays a key role in lysosomal exocytosis by increasing the cytoplasmic Ca^{2+} concentration and promoting the fusion of lysosomes with plasma membrane [35,36]. LY294002, a PI3 kinase inhibitor that can cause inhibition of lysosomes exocytosis [36,37], adhesion of lysosomes to the inner of plasma membrane, induced stagnation of Gly-A7R-NDs inside the cells (Fig. 5B and C). In contrast, ionomycin, an ionophore that transports calcium into the cells and enhances lysosomal exocytosis [38], caused a significant decrease of intracellular fluorescence intensity, only 49% of the control group. Since the lysosomal exocytosis process is energy-dependent, sodium azide significantly inhibited lysosomal exocytosis. The intracellular fluorescence intensity of Gly-A7R-NDs was 1.38 times than that of the control group (Fig. 5C). Gly-A7R-NDs/PTX were also utilized to evaluate the transcytosis. As shown in Fig. 5D, the free inhibitors had ignorable cytotoxicity to the cells at their working concentrations. Lysosomal exocytosis-related inhibitors (especially chloroquin and nocodazole) could significantly enhance the toxicity of Gly-A7R-NDs/PTX to bEnd.3 cells by reducing the exocytosis (Fig. 5E).

Lysosomes are rich of various hydrolases and proteases, and usually considered as the ultimate sites for degradation. Most endocytosed nanoparticles are transported to the lysosomes for elimination. Not only biodegradable polymers such as poly(D,L-lactide-co-glycolide) nanoparticles, but also metal oxide nanoparticles such as iron oxide nanoparticles can be degraded [39–42]. Therefore, strategies for escaping from the lysosomes were preferred for intracellular release of drugs, especially for gene drugs [43–45]. However, nanoparticles such as carbon nanotubes and polystyrene nanoparticles are hardly degraded completely by lysosomes, and excretion occurs parallelly to reduce injury to lysosomes [46,47]. Our results showed evidence that excretion of Gly-A7R-NDs from bEnd.3 cells was generally achieved through lysosomal exocytosis, which might provide new impetus to nanoparticles across the BBB.

4. Conclusion

The transcytosis process of Gly-A7R-NDs involves endocytosis, intracellular trafficking and exocytosis to cross the blood-brain barrier. As summarized in Fig. 6, Gly-A7R-NDs internalized bEnd.3 cells mainly by GLUT-mediated/clathrin dependent endocytosis and macropinocytosis. The intracellular Gly-A7R-NDs remained intact, and were transported out of the cells through Rab11 positive slow recycling endosomes, or by Rab8 positive GLUT4 transport vesicles from golgi apparatus. Gly-A7R-NDs could be delivered to the lysosomes through classic EE-LE-Lysosomes pathway. The main excretion route of Gly-A7R-NDs was lysosomal exocytosis. This work depicted a clear picture of the transcytosis of Gly-A7R-NDs in bEnd.3 cells and revealed the pivotal role of lysosome in this process. Accelerating the rate of lysosomal exocytosis may provide an efficient strategy to improve GLUT-mediated brain targeting drug delivery.

Conflicts of interest

None.

Acknowledgments

This work was financially supported by the National Natural Science Foundation of China (81973245, 81773657, 81673361, 81690263 and 81673370), China Postdoctoral Science Foundation (2019M651385), National Postdoctoral Program for Innovative Talent (BX20190086), Shanghai Municipal Commission of Health and Family Planning (2018BR04), Shanghai Natural Science Foundation (19431900300 and18ZR1404800) and Pudong New Area Commission of Science & Technology (PKJ2016-Y46).

Supplementary materials

Supplementary material associated with this article can be found, in the online version, at doi:10.1016/j.ajps.2020.07.001.

REFERENCES

[1] Agrahari V, Burnouf P, Burnouf T, Agrahari V. Nanoformulation properties, characterization, and behavior in complex biological matrices: challenges and opportunities for brain-targeted drug delivery applications and enhanced translational potential. Adv Drug Deliver Rev 2019;148:146–80.
[2] Pandit R, Chen L, Götz J. The blood-brain barrier: physiology and strategies for drug delivery. Adv Drug Deliver Rev 2019:S169–409.
[3] Deng D, Xu C, Sun P, Wu J, Yan C, Hu M, et al. Crystal structure of the human glucose transporter GLUT1. Nature 2014;510(7503):121–5.
[4] Anraku Y, Kuwahara H, Fukusato Y, Mizoguchi A, Ishii T, Nitta K, et al. Glycaemic control boosts glucosylated nanocarrier crossing the BBB into the brain. Nat Commun 2017;8(1):1001.
[5] Shao K, Ding N, Huang S, Ren S, Zhang Y, Kuang Y, et al. Smart nanodevice combined tumor-specific vector with cellular microenvironment-triggered property for highly effective antiglioma therapy. ACS Nano 2014;8(2):1191–203.
[6] Wang H, Wang S, Wang R, Wang X, Jiang K, Xie C, et al. Co-delivery of paclitaxel and melittin by glycopeptide-modified lipodisks for synergistic anti-glioma therapy. Nanoscale 2019;130:69–77.
[7] Wang H, Wang X, Xie C, Zhang M, Ruan H, Wang S, et al. Nanodisk-based glioma-targeted drug delivery enabled by a stable glycopeptide. J Control Release 2018;284:26–38.
[8] Huang C, Jin H, Qian Y, Qi S, Luo H, Luo Q, et al. Hybrid melittin cytolytic peptide-driven ultrasmall lipid nanoparticles block melanoma growth *in vivo*. ACS Nano 2013;7(7):5791–800.
[9] Dai T, Jiang K, Lu W. Liposomes and lipid disks traverse the BBB and BBTB as intact forms as revealed by two-step Forster resonance energy transfer imaging. Acta Pharm Sin B 2018;8(2):261–71.
[10] Ruan H, Chen X, Xie C, Li B, Ying M, Liu Y, et al. Stapled RGD peptide enables glioma-targeted drug delivery by overcoming multiple barriers. Acs Appl Mater Inter 2017;9(21):17745–56.
[11] Zhang J, Zhang X, Liu G, Chang D, Liang X, Zhu X, et al. Intracellular trafficking network of protein nanocapsules: endocytosis, exocytosis and autophagy. Theranostics 2016;6(12):2099–113.
[12] Zhang J, Chang D, Yang Y, Zhang X, Tao W, Jiang L, et al. Systematic investigation on the intracellular trafficking network of polymeric nanoparticles. Nanoscale 2017;9(9):3269–82.
[13] Reinholz J, Diesler C, Schöttler S, Kokkinopoulou M, Ritz S, Landfester K, et al. Protein machineries defining pathways of nanocarrier exocytosis and transcytosis. Acta Biomater 2018;71:432–43.
[14] Elkin SR, Lakoduk AM, Schmid SL. Endocytic pathways and endosomal trafficking: a primer. Wiener Medizinische Wochenschrift 2016;166(7–8):196–204.
[15] Harisa GI, Badran MM, Alanazi FK, Attia SM. An overview of nanosomes delivery mechanisms: trafficking, orders, barriers and cellular effects. Artif Cells Nanomed Biotechnol 2018;46(4):669–79.
[16] Fröhlich E. Cellular elimination of nanoparticles. Environ Toxicol Phar 2016:4690–4.
[17] Wei X, Zhan C, Shen Q, Fu W, Xie C, Gao J, et al. A D-Peptide ligand of nicotine acetylcholine receptors for brain-targeted drug delivery. Angew Chem Int Ed Engl 2015;54(10):3023–7.
[18] Yang D, Liu D, Qin M, Chen B, Song S, Dai W, et al. Intestinal mucin induces more endocytosis but less transcytosis of nanoparticles across enterocytes by triggering

nanoclustering and strengthening the retrograde pathway. Acs Appl Mater Inter 2018;10(14):11443–56.
[19] Emperador-Melero J, Huson V, van Weering J, Bollmann C, Fischer Von Mollard G, Toonen RF, et al. Vti1a/b regulate synaptic vesicle and dense core vesicle secretion via protein sorting at the Golgi. Nat Commun 2018;9(1):3421.
[20] Pan X, Meriin A, Huang G, Kandror KV. Insulin-responsive amino peptidase follows the Glut4 pathway but is dispensable for the formation and translocation of insulin-responsive vesicles. Mol Biol Cell 2019;30(12):1536–43.
[21] Xu Y, Xu J, Shan W, Liu M, Cui Y, Li L, et al. The transport mechanism of integrin $\alpha_v\beta_3$ receptor targeting nanoparticles in Caco-2 cells. Int J Pharmaceut 2016;500(1–2):42–53.
[22] Dragwidge JM, Scholl S, Schumacher K, Gendall AR. NHX-type Na^+ (K^+)/H^+ antiporters are required for TGN/EE trafficking and endosomal ion homeostasis inArabidopsis thaliana. J Cell Sci 2019;132(7):s226472.
[23] He B, Lin P, Jia Z, Du W, Qu W, Yuan L, et al. The transport mechanisms of polymer nanoparticles in Caco-2 epithelial cells. Biomaterials 2013;34(25):6082–98.
[24] Shan W, Zhu X, Liu M, Li L, Zhong J, Sun W, et al. Overcoming the diffusion barrier of mucus and absorption barrier of epithelium by self-assembled nanoparticles for oral delivery of insulin. ACS Nano 2015;9(3):2345–56.
[25] Grant BD, Donaldson JG. Pathways and mechanisms of endocytic recycling. Nat Rev Mol Cell Bio 2009;10(9):597–608.
[26] Yanes RE, Tarn D, Hwang AA, Ferris DP, Sherman SP, Thomas CR, et al. Involvement of lysosomal exocytosis in the excretion of mesoporous silica nanoparticles and enhancement of the drug delivery effect by exocytosis inhibition. Small 2013;9(5):697–704.
[27] Sipos A, Kim K, Chow RH, Flodby P, Borok Z, Crandall ED. Alveolar epithelial cell processing of nanoparticles activates autophagy and lysosomal exocytosis. Am J Physiol-Lung C 2018;315(2):L286–300.
[28] Sandhof CA, Hoppe SO, Druffel-Augustin S, Gallrein C, Kirstein J, Voisine C, et al. Reducing INS-IGF1 signaling protects against non-cell autonomous vesicle rupture caused by SNCA spreading. Autophagy 2020;16(5):878–99.
[29] Flessner LB, Moley KH. Similar [DE]XXXL[LI] motifs differentially target GLUT8 and GLUT12 in Chinese hamster ovary cells. Traffic 2009;10(3):324–33.
[30] Augustin R, Riley J, Moley KH. GLUT8 contains a [DE]XXXL[LI] sorting motif and localizes to a late endosomal/lysosomal compartment. Traffic 2005;6(12):1196–212.
[31] Schmidt S, Joost H, Schürmann A. GLUT8, the enigmatic intracellular hexose transporter. Am J Physiol Endocrinol Metab 2009;296(4):E614–18.
[32] Chou H, Chuang K, Tsai Y, Chen Y. Genistein inhibits glucose and sulphate transport in isolated rat liver lysosomes. Br J Nutr 2010;103(2):197–205.
[33] Mony VK, Benjamin S, O'Rourke EJ. A lysosome-centered view of nutrient homeostasis. Autophagy 2016;12(4):619–31.
[34] Hall EA, Ramsey JE, Peng Z, Hayrapetyan D, Shkepu V, O'Rourke B, et al. Novel organometallic chloroquine derivative inhibits tumor growth. J Cell Biochem 2018;119(7):5921–33.
[35] Platonova N, Manzo T, Mirandola L, Colombo M, Calzavara E, Vigolo E, et al. PI3K/AKT signaling inhibits NOTCH1 lysosome-mediated degradation. Genes Chromosom Cancer 2015;54(8):516–26.
[36] Tsunemi T, Perez-Rosello T, Ishiguro Y, Yoroisaka A, Jeon S, Hamada K, et al. Increased lysosomal exocytosis induced by lysosomal Ca^{2+} channel agonists protects human dopaminergic neurons from α-Synuclein toxicity. J Neurosci 2019;39(29):5760–72.
[37] Trajkovic K, Jeong H, Krainc D. Mutant huntingtin is secreted via a late endosomal/lysosomal unconventional secretory pathway. J neurosci 2017;37(37):9000–12.
[38] Shen Y, Gu Y, Su W, Zhong J, Jin Z, Gu X, et al. Rab27b is involved in lysosomal exocytosis and proteolipid protein trafficking in oligodendrocytes. Neurosci Bull 2016;32(4):331–40.
[39] Zeng J, Shirihai OS, Grinstaff MW. Degradable nanoparticles restore lysosomal pH and autophagic flux in lipotoxic pancreatic beta cells. Adv Healthc Mater 2018;8(12):1801511.
[40] Bourdenx M, Daniel J, Genin E, Soria FN, Blanchard-Desce M, Bezard E, et al. Nanoparticles restore lysosomal acidification defects: implications for Parkinson and other lysosomal-related diseases. Autophagy 2016;12(3):472–83.
[41] Wu M, Gu L, Gong Q, Sun J, Ma Y, Wu H, et al. Strategies to reduce the intracellular effects of iron oxide nanoparticle degradation. Nanomedicine 2017;12(5):555–70.
[42] Volatron J, Carn F, Kolosnjaj-Tabi J, Javed Y, Vuong QL, Gossuin Y, et al. Ferritin protein regulates the degradation of iron oxide nanoparticles. Small 2017;13(2):1602030.
[43] Zylberberg C, Gaskill K, Pasley S, Matosevic S. Engineering liposomal nanoparticles for targeted gene therapy. Gene Ther 2017;24(8):441–52.
[44] Xu J, Liu Y, Li Y, Wang H, Stewart S, Van der Jeught K, et al. Precise targeting of POLR2A as a therapeutic strategy for human triple negative breast cancer. Nat Nanotechnol 2019;14(4):388–97.
[45] Joris F, De Backer L, Van de Vyver T, Bastiancich C, De Smedt SC, Raemdonck K. Repurposing cationic amphiphilic drugs as adjuvants to induce lysosomal siRNA escape in nanogel transfected cells. J Control Release 2018;269:266–76.
[46] Chu Z, Huang Y, Tao Q, Li Q. Cellular uptake, evolution, and excretion of silica nanoparticles in human cells. Nanoscale 2011;3(8):3291–9.
[47] Popp L, Tran V, Patel R, Segatori L. Autophagic response to cellular exposure to titanium dioxide nanoparticles. Acta Biomater 2018:79354–63.